Soil Dynamics and Earthquake Engineering 204 (2026) 110192

Contents lists available at ScienceDirect

Soil Dynamics and Earthquake Engineering

journal homepage: www.elsevier.com/locate/soildyn

The influence of fabric and mineralogy on the dynamics of carbonate silty clays

Alain Conrado-Palafox *, Timothy Newson

Geotechnical Research Centre, Department of Civil and Environmental Engineering Western University, London, N6A 5B9, Canada

ARTICLE INFO

Keywords:
Carbonate soils
Clay
Shear modulus
Damping ratio
Stiffness degradation
Soil fabric

ABSTRACT

The Gulfs of Mexico and Texas represent promising locations for offshore wind farms due to their favourable wind conditions. However, the presence of calcareous silts and carbonate clays along the Florida and Yucatan coasts pose significant geotechnical challenges for dynamic foundation systems. While the dynamic properties of sands and natural clays are relatively well established, the role of carbonate silt inclusions in clay matrices is less well defined. In this study, artificial soils were utilized to control fabric trough variations in silt fractions and mineralogy. These mixtures blended a high plasticity lacustrine clay with calcium carbonate particles (aragonite and calcite) and silicate silt particles. Dynamic soil properties were determined through isotropically consolidated triaxial tests with vertical bender elements and resonant column measurements over a wide strain range. The shear modulus measurements for these artificial carbonate mixtures show good agreement with clayey silt mixtures from tests on other offshore marine sediments from the literature. Relative to reconstituted Ottawa clay, at pressures of 100 kPa, the shear modulus normalized for void ratio increased by 34% for aragonite mixtures, compared to 6% for silicate mixtures. At reference strain levels, the 50% aragonite mixture showed a 6% stiffness increase, whereas the 50% silicate mixture exhibited reductions of up to 38%. Lower damping was also observed in mixtures with higher clay contents. The results indicate that the plasticity index and grading heterogeneity significantly influenced the mechanical responses, with the aragonite-clay mixtures showing more clay-like behaviour, and silicate-clay mixtures showing more sand-like behaviour.

1. Introduction

Despite extensive studies of the dynamic behaviour of many types of soils and the availability of associated empirical design equations, the shear moduli and damping ratios of intermediate carbonate soils, such as silty clays, remain less well characterized due to their complex mineralogy, fabric, and particle interactions. Most existing studies have focused on natural clays, cohesionless soils and soils from specific sites, limiting their general applicability [1,2]. Laboratory methods, including isotropically consolidated triaxial tests with bender elements and resonant column measurements, have previously been employed to characterize dynamic properties at strains from 0.00001% to 0.1%. Empirical models, such as hyperbolic formulations, are commonly used to represent strain-dependent stiffness changes and reduce the need for extensive site-specific investigations [3–7].

Numerous studies have examined the small-strain stiffness of fine-grained soils through laboratory testing and early work on terrigenous clays established that the maximum shear modulus (G_{max}) depends strongly on the effective stress, void ratio, and plasticity [3–7]. Although widely applied in design, derived empirical formulations are inherently linked to the mineralogy and structure of silicate soils and their applicability to carbonate materials remains uncertain. Unlike sands, where particle size distributions can often be used to establish predictive correlations, clays often show greater variability due to bonding, fabric and particle mineralogy factors, making simple generalizations difficult [8].

In fine-grained soils, it is well-established that slightly sensitive natural clays with low plasticity and liquid limits tend to exhibit higher maximum shear modulus (G_{max}) values than high plasticity clays [3–7]. Low compressibility silt grain assemblages show higher shear wave velocities than more compressible fine soil skeletons [9], and an increase in silt content in clean sands often reduces stiffness. These tendencies are attributed to the replacement of strong interparticle contacts with more deformable and weaker contacts [10,11]. The behaviour of intermediate soils containing clay and carbonate silt is not well understood. A key

Present address: Spencer Engineering Building, Rm. 3084, London, Ontario, Canada, N6A 5B9.
* Corresponding author.
E-mail addresses: aconrado@uwo.ca (A. Conrado-Palafox), tnewson@eng.uwo.ca (T. Newson).

https://doi.org/10.1016/j.soildyn.2026.110192
Received 23 November 2025; Received in revised form 28 January 2026; Accepted 10 February 2026
Available online 19 February 2026
0267-7261/

transition occurs when the clay fraction becomes the dominant stress-carrying matrix, with silt particles beginning to act as passive inclusions [12]. Studies on liquefaction susceptibility show that silt contents above 12% to 30% can separate coarse particles and shift the mechanical behaviour to that of a fines-controlled material, particularly when the fines are of low plasticity index (PI $<$ 12%) and governed only by interparticle friction [13]. However, identifying this transition threshold is complicated by the influence of mineralogy, gradation, particle shape, and fabric [14]. This change is even less well understood when the silt fraction is composed of calcium carbonate minerals. Studies have shown that clays with higher plasticity index, carbonate content and overconsolidation ratios have greater small-strain stiffness (G_{max}) [15–17]. Although these works suggest that both plasticity and the presence of carbonates influence G_{max}, it is still difficult to determine which factors play the most significant roles.

The reduction of shear modulus and the associated increase in damping ratio with strain have also been well documented for terrigenous fine-grained soils. Classical hyperbolic models [7,18,19] effectively capture this non-linear behaviour. To better interpret these models and their parameters, it is essential to understand the underlying mechanisms that govern stiffness and damping in fine-grained soils. The stiffness and damping behaviour of fine-grained soils are predominantly governed by a combination of physicochemical and mechanical factors that modify the interparticle bonding, contact stiffness, and energy dissipation.

Based on the work of previous authors, the relative importance of various factors can be summarized as follows. The plasticity index shows strong control of the shape and position of the stiffness degradation and damping curves. The soil structure or sensitivity has a comparable influence, particularly for sensitive clays, where interparticle electrochemical bonding leads to higher initial stiffness and reduced damping [8]. For carbonate fine-grained soils, the combined effect of fabric and interparticle bonding of the calcium carbonate ($CaCO_3$) produces higher small-strain stiffness, and slightly lower damping ratios [17]. Confinement pressure acts as a secondary control, increasing stiffness mainly in low plasticity or non-plastic materials, while its influence becomes less pronounced for highly plastic or structured clays. Finally, the initial void ratio (e_0) and mineralogical composition modulate these effects, with denser and coarser matrices (lower e_0) showing stiffer responses and lower damping. However, literature relationships are predominantly calibrated with marine or alluvial clays of terrigenous origin. Offshore calcareous clays show distinct reference strains and damping ratios because of their microstructural features, suggesting that extrapolating existing empirical relationships may not be appropriate without specific testing confirmation [20].

Although the Gulfs of Mexico (GOM) and Texas have been identified as having particularly suitable offshore areas for wind production, the presence of large zones of carbonate soils provide challenging foundation design conditions [21]. Characterising dynamic properties such as small-strain shear modulus (G_{max}), stiffness degradation (G/G_{max}), and damping ratio (D) will be critical for the evaluation of liquefaction potential and the prediction of dynamic soil-structure interaction (SSI) for many of the required structures and foundations. This includes the lateral response of offshore and other cyclically loaded pile foundations governed by SSI, which are typically modeled using *p-y* curves. Recently, the classical *p-y* curve approach has been improved to create a more efficient design method taking into account the G_{max} of the soil and the rigidity of the piles [22]. Researchers have also recently added the non-linear reduction of stiffness with strain to this approach [23]. However, the dynamic properties for the SSI analysis of suitable offshore gravity and caisson foundations for these wind turbines [24] in the Gulf of Mexico will require knowledge of dynamic behaviour and characterizations of carbonate soils that does not currently exist.

This gap in the literature shows the importance of better understanding the behaviour of these intermediate carbonate soils and the grain mixtures that cause transitions in their behaviour. The current knowledge and frameworks required to predict the dynamic behaviour of carbonate silty clays are lacking and given the importance of this information for the development of future offshore energy infrastructure in the Gulf of Mexico, this needs to be urgently addressed.

2. Study aims

This research aims to evaluate variations in the shear modulus (G_{max}) for very small-strains and the non-linear stiffness degradation and damping behaviour (G/G_{max} and D) for a structured illite clay containing different carbonate and silicate silt sized inclusions. This approach has enabled a controlled investigation of the effect of carbonate content on small-strain stiffness, while preserving a realistic representation of offshore fine-grained carbonate clay to silt sediments. The shear modulus variation is analyzed in relation to plastic index, compressibility index, grain size distribution, and gap-graded soil characteristics, to improve the understanding of how soil state parameters influence the shear modulus and damping behaviour. Additionally, the findings shown in this paper highlight key considerations for applying different commonly used predictive models.

3. Materials

Ottawa clay was selected to create artificial carbonate clayey samples due to its glaciolacustrine characteristics and mineralogical similarity to marine sediments. Illite, which is the second most abundant mineral in the Gulf of Mexico and decreases in concentration from shallow to deep waters [25], is the dominant mineral in Ottawa clay. This lacustrine clay from Eastern Canada also contains traces of kaolinite and is classified as a sensitive material. *In-situ*, this clay has an average 80% water content and a liquidity index around 2.0 with an overconsolidation ratio (OCR) of 2.55. The material has a plastic limit (PL) of 30% and a liquid limit (LL) of 53% with a saturated density (ρ_{sat}) of 1.53 g/cm^3 and a specific gravity (G_s) of 2.77, as shown in Table 1.

Artificial soils were created with two different $CaCO_3$ silt grain forms blended into the clay mixtures (synthetic calcite and crushed aragonite). Calcite particles were created using the precipitation synthesis method described by Yu et al. [26], with a solution of sodium carbonate Na_2CO_3 (5 mol) in 100 ml of poly styrene-alt-maleic acid PSMA (1 g/L). The pH was adjusted to 10 with hydrochloric acid HCl. A calcium chloride $CaCl_2$ (5 mol) solution was then added whilst agitating the solution with a magnetic stirrer. The aragonite particles were obtained from crushing fine sand to make particles smaller than 0.075 mm from larger oölitic aragonite sand grains from The Bahamas (distributed by AQUA NATURAL). Further tests were performed with a commercial silicate silt Sil-Co-Sil-106, which is a sub-angular ground quartz. Nine artificial clayey silt mixtures were created to conduct dynamic tests with 25%, 50% and 60% calcite, aragonite and silicate particles by weight.

Table 1
Clay and artificial calcareous and carbonate clayey silt properties.

Sample	G_s	PI (%)	LL (%)	e_0	e_0/e_L	ρ_{sat} (g/cm^3)	λ
Undisturbed clay	2.77	27.2	54.0	2.32	1.55	1.53	0.483
Reconstituted clay	2.77	27.2	54.0	1.27	0.85	1.77	0.105
25% silicate	2.74	10.7	42.5	1.08	0.93	1.83	0.083
50% silicate	2.71	5.5	33.3	0.86	0.96	1.92	0.058
60% silicate	2.7	2.5	28.7	0.91	1.16	1.89	0.059
25% calcite	2.75	13.4	48.0	1.25	0.95	1.77	0.093
50% calcite	2.73	9.5	38.0	1.01	0.98	1.86	0.087
60% calcite	2.72	9.0	35.5	0.91	0.89	1.90	0.079
25% aragonite	2.81	12.3	42.0	1.14	0.96	1.84	0.095
50% aragonite	2.86	10.3	36.0	1.01	0.98	1.92	0.077
60% aragonite	2.87	7.3	31.4	1.01	1.03	1.93	0.076

3.1. Mixture preparation

These materials were initially mixed in slurry form at water contents close to 1.5 times their liquid limit (e_L = void ratio at liquid limit); this was deemed to be sufficient to easily create samples without particle segregation occurring. Subsequently, the samples were reconstituted in a non-standard long one-dimensional (1-D) oedometer column. The final vertical consolidation pressure was 100 kPa, corresponding to the vertical yielding stress determined from consolidation tests conducted on the undisturbed Ottawa clay sample, and was used to provide an overconsolidation ratio (OCR) close to the undisturbed clay sample (≈2.0), to mimic both lacustrine and marine sediments. The void ratio (e_0) after 1-D consolidation in the long oedometer was used to characterize the initial state of the reconstituted samples.

Before the next stage of laboratory stress-strain tests, the silicate mixtures were found to be a normalized void ratio, e_0/e_L, of approximately 1.01, and the calcite and aragonite mixtures ranged between e_0/e_L = 0.94 and 0.99. These corresponded to saturated densities from ρ_{sat} = 1.77 - 1.93 g/cm^3. It should be noted that no significant time-dependent carbonate cementation bonding was expected, as the samples remained under vertical consolidation for only 24 h. This period was expected to be sufficient for dissipation of excess pore pressures, but too short for any measurable carbonate cementation to develop. The applied consolidation pressure of 100 kPa effectively expelled most of the free pore water, leaving the samples in a firm, mechanically stable state. Owing to the high proportion of Ottawa clay in the mixtures, the reconstituted soils showed sufficient solidity after consolidation, to behave like lightly overconsolidated materials.

3.2. Mixture properties

The specific gravities (G_s), plastic index (PI), liquid limits (LL), saturated density (ρ_{sat}), and corresponding initial void ratios (e_0) of the various samples are shown in Tables 1 and in addition of the virgin compression slope (λ), determined during the isotropic consolidation tests. The index and isotropic compressibility properties of the Ottawa clay mixtures highlight the contrast between the silicate and carbonate inclusions. While the undisturbed clay shows high plasticity (PI = 27%) and a high compression slope $\lambda = 0.48$, a reduction to $\lambda = 0.10$ occurs for the reconstituted sample due to the destruction of the undisturbed fabric and has an associated reduction in the void ratio due to the reconstitution process. The addition of silicate silt abruptly reduces the plasticity (PI < 11%) and leads to lower compressibility (λ = 0.083 - 0.059). In contrast, carbonate inclusions (calcite and aragonite) result in intermediate plasticity values (PI < 13.5%) and higher compressibility (λ = 0.094 - 0.077) compared with the silicates. These findings indicate that carbonate mixtures retain higher compressibility despite reduced plasticity, reflecting the distinctive role of the carbonate mineralogy in modifying the soil fabric and the resulting mechanical behaviour.

The particle size distributions of these mixtures are shown in Fig. 1, and have curves which lie within representative clay and sandy silt grading ranges found in the Bay of Campeche [27]. Fig. 2 shows the coefficient of uniformity (C_u) and the mean particle size (d_{50}) of each mixture. The pure Ottawa clay has a coefficient of uniformity of C_u = 2.08. These values change with silt increments; the 60% calcite mixture has the highest C_u = 27.78, whereas the 60% aragonite mixture has much lower value of C_u = 9.03. The calcite mixtures have the largest grains, while the silicate mixtures lie between the two carbonate forms, according to the mean particle size (d_{50}) shown in Fig. 2.

3.3. Experimental program

The undisturbed and reconstituted clay samples and the nine artificial mixtures were initially used to determine the relationship between the small-strain shear modulus, $G_{\max}$, and confining pressure using bender elements (BE). Stiffness reduction and damping ratios with strain

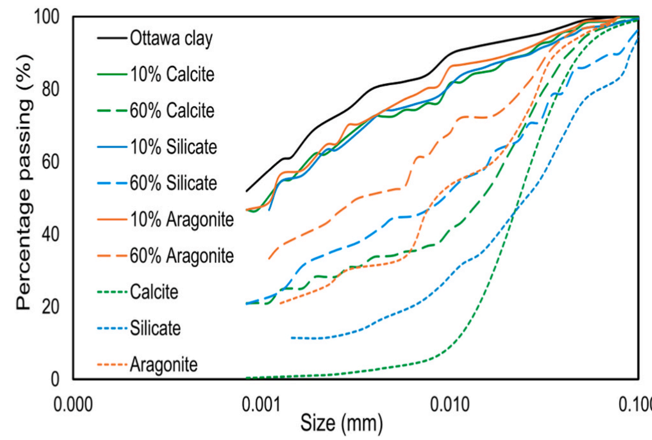

Fig. 1. Particle size distribution of samples.

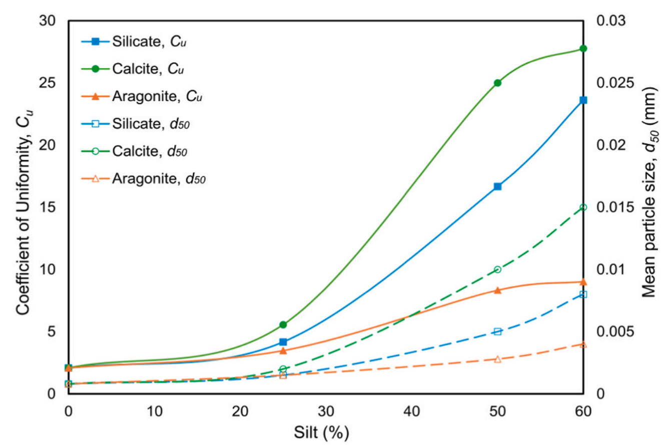

Fig. 2. Particle size distribution curve characteristics: mean particle size, d_{50} and coefficient of uniformity, C_u for the artificial mixtures.

were also determined in a resonant column (RC). For the BE tests, the formed cylindrical samples (5 cm × 10 cm) were saturated and allowed to swell isotropically in a Bishop and Wesley triaxial cell at stresses <50 kPa. After achieving Skempton's pore pressure parameter (B) values larger than 0.95, further isotropic consolidation stages were applied up to 800 kPa. At each confining pressure (σ_m'), vertical bender element (BE) tests were performed to find the shear wave velocity (v_s). The resonant column samples were back-pressure saturated to 140 kPa and isotropically consolidated in a secondary compression stage to 60, 100 and 300 kPa. The samples were maintained under the target confining pressure for a 24-h consolidation period, prior to initiating measurements of shear modulus and damping ratio.

3.4. Bender element testing

The maximum shear modulus ($G_{\max}$) or shear modulus at extremely small-strains (i.e. γ = 0.0001% or 0.001%) was determined using very low strain shear wave propagation, assumed not to modify the fabric of the sample [10]. $G_{\max}$ was obtained thorough eq. (1):

$$G_{max} = \rho * v_s^2 \tag{1}$$

Where ρ is the bulk density in kg/m^3 and v_s is the shear wave velocity in m/s. Equation (1) is a consequence of the influence of the packing state (the porosity, density, etc.) and the contact number (shear wave propagation efficiency) of the soil grains [10].

Shear wave velocities (v_s) were obtained using vertical bender element readings, along with measured distances between the source and the received waveforms using eq. (2):

$$v_s = \frac{L}{\Delta t} = \frac{L}{\left(\Delta t_{start\ arrival} + \Delta t_{peak-peak}\right)/2} \quad (2)$$

Where Δ_t is the average of the first and peak arrival or the time to start arrival, and v_s is the shear wave velocity in m/s. L is the height of the sample in m, which corresponds to the tip-to-tip distance between the bender elements.

The travel time distance Δ_t, shown in Fig. 3, was obtained from time domain analysis, taking the average reading of the (A) first deflection, (B) first bump maximum, (C) zero crossing and (D) major first peak [28]. The data processing of the time histories, cross-correlations and frequency domain plots were carried out with the GDS bender element test analysis tool [29].

Based on recommendations in the literature [28,30,31], single-cycle sinusoidal signals with input frequencies between 2 and 8 kHz were sequentially tested for each confining stress. This frequency range was selected to explore different combinations of wavelength, and to identify the excitation that produced a ratio of specimen length to wavelength, $L/\lambda > 2$, while maintaining a clear and stable time domain response. This analysis allowed the verification of whether the frequency domain response showed the expected linear trend in phase angle-frequency space, which is characteristic of a robust transfer function [28,30,31].

Fig. 4 shows two representative time-domain plots obtained at confining stresses between 15 and 500 kPa for the 25% and 60% aragonite mixtures. These examples illustrate the typical evolution of the received waveform and the identifiable sequence of first deflection and major first peak. As expected, the arrival time systematically decreases with increasing confining pressure and with higher silt contents. Furthermore, maintaining $L/\lambda > 2$ required increasing the input frequency as the confining pressures increased.

Fig. 5 shows two examples of the corresponding frequency-domain outputs, including the input-output spectra and the unwrapped phase relationships. The phase angle-frequency curves show the standard behavior expected for BE testing: a dominant energy band centered near the transmitted frequency and a largely linear phase trend across the active spectral region. These outputs were used to verify that the transmitted frequency produced a stable response consistent with previous BE studies [28,30,31].

3.5. Resonant column testing

The GDS resonant column (RC) is a Stokoe type, where the base of the sample is fixed, and the applied torsional excitation occurs at the free top of the sample [32]. The shear modulus for small and up to medium strains (0.001% - 0.1%) were found using this apparatus. The resonant frequency (f_n) was determined by applying torsional excitation from 30 to 120 Hz to the sample and selecting the frequency for the maximum amplitude obtained in millivolts (mV) according to the ASTM standard [33]. The preliminary range of frequency values were selected based on the shear wave velocity results obtained from the bender elements performed in previous tests, to provide a maximum shear modulus for small-strain in the resonant column. This procedure was selected because the shear strain on the specimen is not constant for all

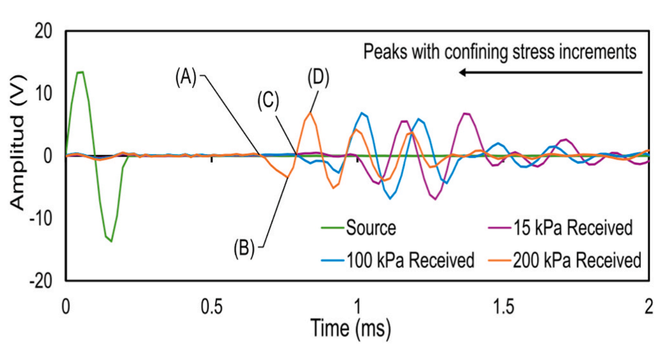

Fig. 3. Results of typical bender element tests on the reconstituted samples.

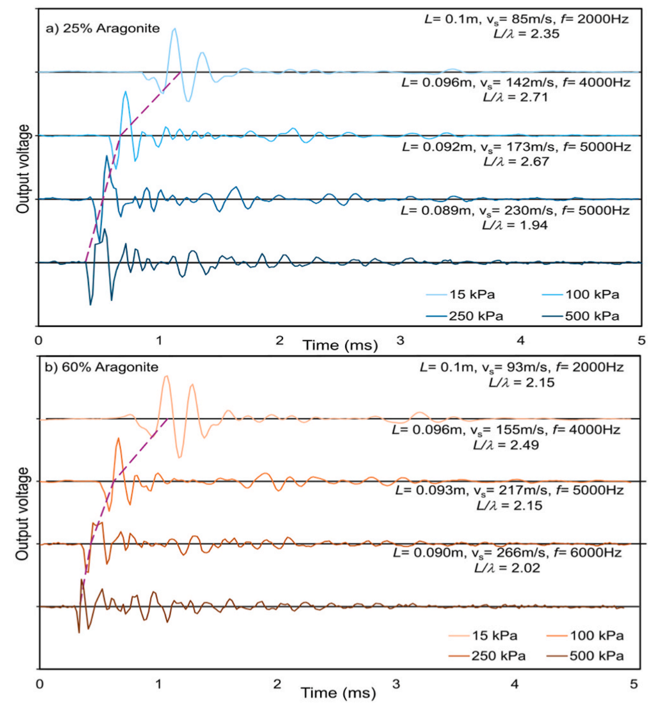

Fig. 4. Determination of the arrival time for the 25% and 60% aragonite mixtures for different stresses.

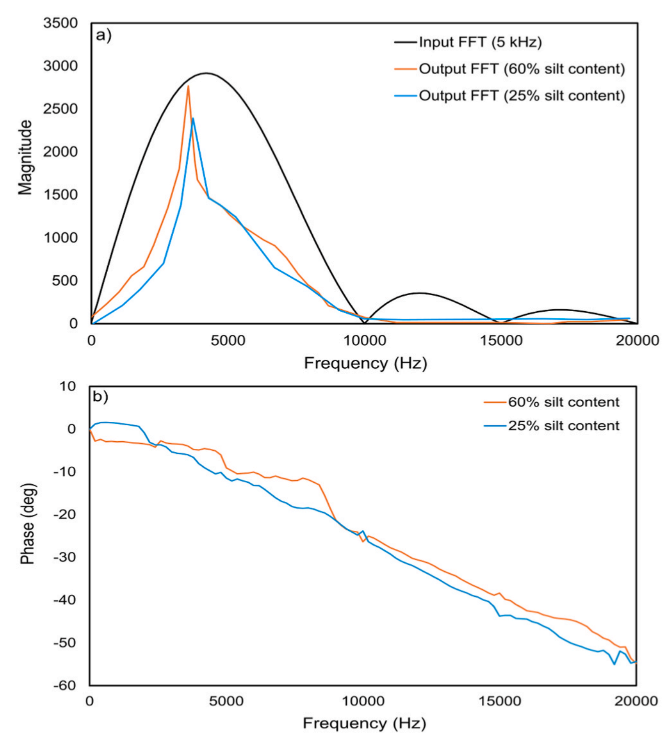

Fig. 5. Frequency domain outputs for the 25% and 60% aragonite mixtures at 250 kPa.

frequencies, potentially leading to over/under estimation in resonant frequencies [34].

The shear modulus (G) was obtained from the v_s values for each natural frequency (f_n) at specific shear strains (γ). Following the theory of wave propagation and the solution for the equation of motion for fixed-free resonant column devices [35], the v_s values were determined using eqs. (3) and (4). These were transformed into shear modulus values using eq. (1).

$$v_s = \frac{2*\pi*f_n*H}{\sqrt{I/I_0}} \quad (3)$$

$$\frac{I}{I_0} = \left(\frac{f_n*H}{v_s}\right)*tan\left(\frac{f_n*H}{v_s}\right) \quad (4)$$

Where H is the height of the sample in m, f_n is the natural frequency in Hz, I is the mass polar moment of inertia of soil specimen in kg*m^2, and I_0 is the mass polar moment of inertia of resonant column drive system in kg*m^2. I_0 was determined using the conventional calibration method with standard aluminium bars [32,36]. The measured velocities of each aluminium bar fall within ±3% of the reference value, confirming the reliability of the calibration. Similarly, these results are comparable with those reported previously by other authors [37,38].

The viscous damping ratio was determined from the free vibration decay shape curve and then found numerically from the logarithmic decrement equation. First the logarithmic decrement (δ) is provided by the best straight line fit slope of the peak amplitude – cyclic number plot, and then viscous damping ratio is determined using δ according to eq. (5). The number of cycles used for the analysis is commonly taken between 10 and 50 [39].

$$D\ (\%) = \sqrt{\frac{\delta^2}{4*\pi^2 + \delta^2}} \quad (5)$$

4. Results and discussions

4.1. Shear wave velocity (v_s)

Fig. 6 shows the shear wave velocity (v_s) for different confining pressures (σ_m') for the undisturbed and reconstituted pure Ottawa clay. As the figure indicates, the shear wave velocities for the undisturbed samples have lower values than the reconstituted samples, since the reconstituted samples have lower initial void ratios (e_0), which leads to a reduced porosity. Consequently, shear waves propagate faster due to the contact number increasing within the reconstituted sample compared to the undisturbed sample. The relationship between shear wave velocity (v_s) and effective confining stress (σ_m') is often characterized with the exponential relationship [40], expressed in eq. (6):

$$v_s = \alpha*\left(\sigma_m'/P_0\right)^{\beta} \quad (6)$$

Where factor α and *β-exponent* are fitting parameters and P_0' is a reference stress (1 kPa).

However, determining the fitting parameters α and *β-exponent* in sensitive clays can be challenging due to the influence of natural soil structure and sensitivity, previous and initial confining stresses, electromechanical interactions, and the high specific surface area of clay particles [41]. These factors, combined with the interface of compressive waves in the selection of shear wave arrivals and the effects of the excitation frequency on the measured wave velocity (thereby influencing the initial small-strain stiffness), can lead to variability in the estimated shear wave velocities [34,42].

Fig. 6 also shows the shear wave velocity behaviours of some of the artificial silty clay mixtures and Table 2 shows the associated factor α and *β-exponents* for each curve. The 25% silicate, calcite and aragonite mixtures lie in the same range as the normally consolidated

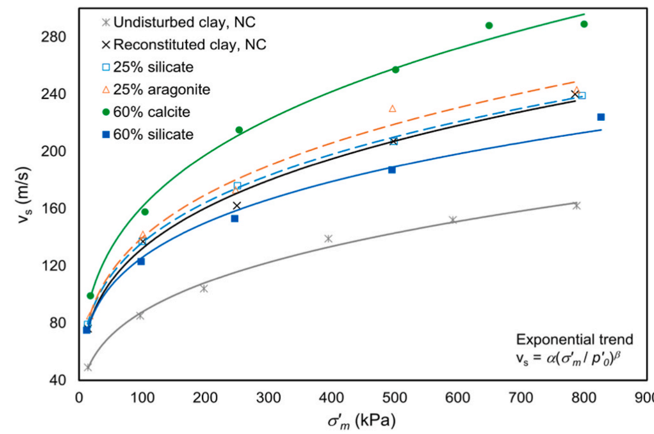

Fig. 6. Shear wave velocities v_s for undisturbed and reconstituted Ottawa clay samples and some artificial mixtures.

reconstituted clay sample. There is an increase in factor α with the addition of the silt particles, while there is a slight reduction in the *β-exponent*; with these two changes the final shear wave velocity relationship has a curve similar to the reconstituted clay sample. On the other hand, for the 50% calcium carbonate silt contents (aragonite and calcite), there is a slight variation in factor α and *β-exponent*, showing an increase in the shear wave velocity, which results in the curve lying above the reconstituted clay sample. However, the 50% silicate content also has a decrease in the *β-exponent*, thereby reducing the shear wave velocity. This pronounced reduction in the β-exponent, observed when increasing silicate contents from 25% to 50% - 60%, reflects a transition toward a contact network dominated by silicate silt particles with limited physicochemical interaction, resulting in a weaker dependence of stiffness on the effective stress. The potential underlying mechanisms governing contact rearrangement are discussed in the following section.

4.1.1. Effect of mineral composition on fitting parameters α and β

Combination of these two fitting parameters have been identified for different soils by previous researchers [9,11,43–50], and this characterization is shown in Fig. 7. The low factor α and high *β-exponent* for the undisturbed clay sample lie within the pure clay behaviour zone, according to the α and *β-exponent* relationship [9,44] in Fig. 7. This result is associated with the high initial porosity and pronounced compressibility of the undisturbed sensitive clay during loading [51]. In contrast, the reconstituted Ottawa clay lies within the clay to silt behaviour due to its relatively high factor α, likely influenced by fabric densification during the 1-D consolidation at 100 kPa, and more limited v_s resolution at low stresses [52].

Both the carbonate and silicate mixtures lie within the clay to silt behaviour zone, shifting toward a silt to sand trend as the silt content increases. The main difference for the calcium carbonate mixtures is that they show higher *β-exponent* values than the silicate mixtures, which is

Table 2
Factor α and *β-exponent* values of artificial clayey silt mixtures.

Sample	Factor α (m/s)	*β-exponent*	R^2
Reconstituted clay	36.41	0.2789	0.9927
25% silicate	39.35	0.2700	0.9992
50% silicate	39.80	0.2594	0.9989
60% silicate	39.17	0.2530	0.9921
25% calcite	41.51	0.2783	0.9867
50% calcite	41.19	0.2749	0.9848
60% calcite	42.08	0.2918	0.9937
25% aragonite	38.57	0.2795	0.9871
50% aragonite	39.11	0.2926	0.9945
60% aragonite	41.65	0.2940	0.9936

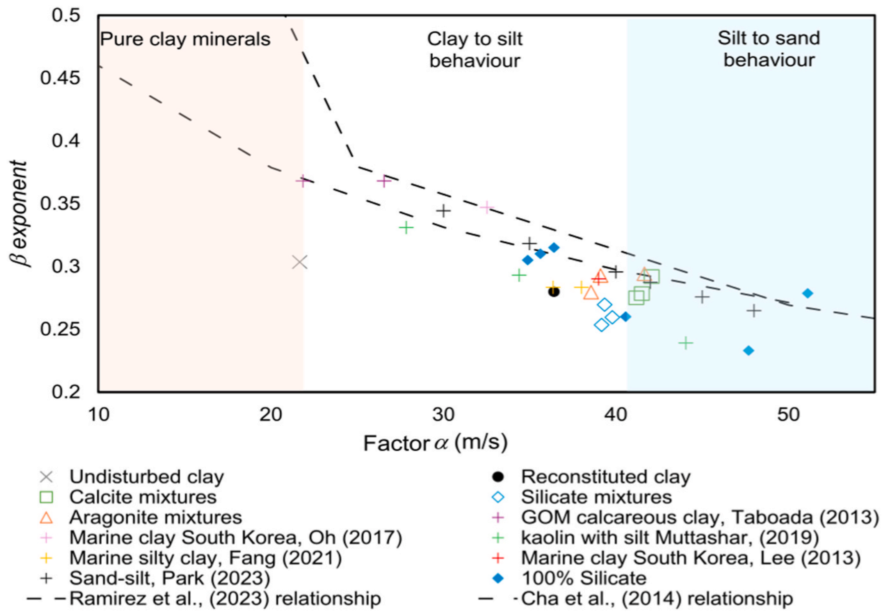

Fig. 7. Factor α and β - *exponent* relationship according to Cha et al. [9] and Ramirez et al. [44].

also beneficial for liquefaction susceptibility [13]. This reflects the role of the calcium (Ca^{2+}) ions, which contract the diffuse double layer, reduce electrochemical repulsion, and strengthen interparticle contacts [53,54]. This mechanism promotes rigid particle networks through physicochemical, non-frictional interactions by contracting the diffuse double layer, rather than true crystalline cementation, increasing shear wave velocities. Silicate silt particles, with low surface area and minimal electrochemical activity, develop weaker contacts and limited stiffness gain with stress, resulting in smaller β-exponent values [55].

The observed differences between the undisturbed clay and the reconstituted clay and artificial mixtures highlight the role of structural degradation in governing the dynamic response of the soil mixtures. While the intact clay retains a natural, metastable fabric associated with structure, sensitivity, and stress-dependent stiffness, this structure is largely destroyed during remolding and reconstitution. Consequently, the artificial and reconstituted clay mixtures behave as mechanically stable, non-structured materials, dominated by particle rearrangement and densification during the consolidation, thereby limiting the influence of any structure on the small-strain stiffness.

4.1.2. Comparative results with other binary soils

The artificial calcium carbonate mixtures show factor α values 11% - 15% higher and β-*exponents* $\approx$ 4% higher than the reference reconstituted clay (α = 36, β = 0.28), aligning with moderate plasticity offshore marine silty clays [45,46], which are also shown in Fig. 7. In contrast, other marine calcareous clays [43,47] show reduced factor α values by −21% and β-*exponent* increased by 28%, reflecting strong stress-dependent shear stiffness due to collapse of the open, metastable microstructure and high compressibility of diatom particles. From all of these results and comparisons it can be seen that factor α decreases with increasing plasticity index, clay fraction, and compressibility index (C_c), although mineralogy and microstructure cause deviation from linear trends [48,49]. Pure silica silt samples display highly variable shear wave velocity fitting parameters, indicating complex dynamic behaviour [11,50].

Despite the fact that Ottawa clay is illite and mineralogically consistent with many Gulf of Mexico marine sediments, its high sensitivity originates from a glaciolacustrine depositional history, resulting in a metastable fabric that may differ from the metastable structures typically observed in offshore marine clays due to salt flocculation. As a result, the contrast observed between the undisturbed and reconstituted Ottawa clay represents a pronounced case of structural degradation, rather than a direct analogue for all marine clay conditions. In this study, the undisturbed Ottawa clay is therefore used as a reference material to isolate and quantify the influence of soil structure on the dynamic response, while the reconstituted clay and artificial mixtures represent mechanically homogenized states in which structural effects are minimized. Consequently, the observed differences should be interpreted as bounding the potential impact of destructuration on dynamic properties, rather than implying direct equivalence with *in-situ* Gulf of Mexico sediments.

4.2. Maximum shear modulus (G_{max})

Fig. 8 shows the values of G_{max} determined from the bender element v_s readings against void ratio (e), exhibiting trends similar to those found by Li et al. [56] for gap-graded soils; as the silt content increases, these relationships shift to the left. Although these curves are informative, it is difficult to isolate the effect of packing density on G_{max}, since the global void ratio (e) is not constant; shear modulus varies with changes with silt content (particle size ratios, R_d and coefficient of uniformity, C_u) and plasticity (PI).

The observed increase in G_{max} with silt content is attributed to different micromechanical mechanisms that depend on the mixture compositions. At low silt content (25%), the increase in G_{max} is primarily associated with partial densification of the clay matrix. At higher silt contents (50% and 60%), the increase in G_{max} is mainly governed by the reinforcing contribution of the silt particles, which progressively participate in load transfer.

From a conceptual threshold coarse content (CC_{th}) perspective, coarse grain (silt) contacts play a primary role when the fine content (FC) is lower than CC_{th}. Conversely, when FC exceeds the threshold fines content (FC_{th}), fine grain contacts progressively dominate the mechanical response, while coarse grains become dispersed within the matrix and provide only secondary reinforcement until complete separation occurs [57]. Based on eq. (7), the FC_{th} of the artificial mixtures is approximately 74% (corresponding to 26% silt), representing the minimum clay content at which inter-fine grain contacts govern the response. The CC_{th} of the artificial mixtures is approximately 65%, estimated using representative maximum void ratios for the silt fractions

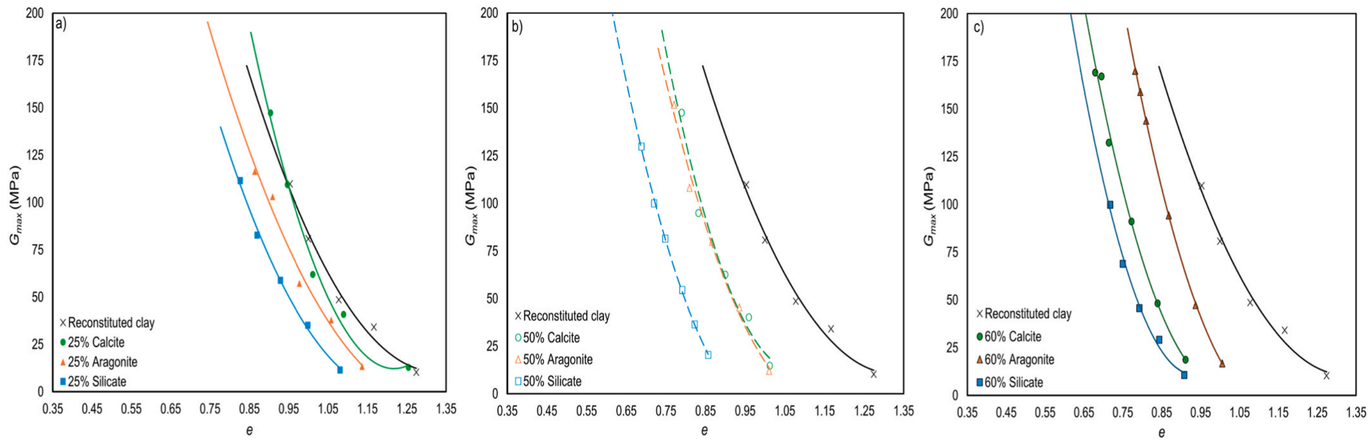

Fig. 8. Shear modulus (G_{max}) against void ratio (e).

($e_{max} = 1.4$ for calcite and aragonite, and 1.2 for silicate) and defining the maximum void ratio of the clay as e_L, following the approach proposed in eq. (8) [58]. Accordingly, the 50% and 60% mixtures fall within the transition regime between inter-fine grain and inter-coarse grain contact dominance.

Further insight is obtained by examining the inter-fine void ratio, e_f, defined in eq. (9). Relative to the pure clay ($e_f = 1.74$), e_f decreases at 25% silt content (average $e_f \approx 1.57$), indicating partial densification of the clay matrix. At higher silt contents (50% and 60%), e_f increases again, accompanied by a reduction in the inter coarse void ratio, e_c, defined in eq. (10). Consistent with the framework proposed by Thevanayagam et al. [57], the increase in e_f reflects a progressive reduction in load transfer through fine grain contacts and a corresponding increase in the contribution of silt contacts.

$$FC_{th} = \frac{e_c}{1 + e_c + e_f} \tag{7}$$

$$CC_{th} = (1 + e_{max}) / (e_{max} + 1 + e_L) \tag{8}$$

$$e_f = V_v / V_f \tag{9}$$

$$e_c = (V_v + V_f) / V_c \tag{10}$$

Where FC_{th} is the threshold fines content, CC_{th} is threshold coarse content, e_c is the intergranular coarse (silt) void ratio, e_f is the inter-fine (clay) void ratio, V_v is the void volume, V_f is the fine (clay) volume, V_c is the coarse (silt) volume, and e_{max} is the maximum void ratio [57,58].

4.2.1. Transition of G_{max} in gap-graded soils

While void ratio is an effective physical index to evaluate G_{max}, the particle size distributions may also provide a reliable indicator for cohesionless soils [59]. In contrast, for cohesive soils such as silty clays, it is necessary to account for interparticle (non-frictional) bonding forces due to the plasticity, which can significantly influence the mechanical behaviour [46]. The small-strain stiffness G_{max} was evaluated under a reference state to investigate the influence of mixture consistency and packing on the dynamic behaviour of the mixtures. A constant void ratio of $e = 0.8$ was selected, which corresponds to a stiff-plastic consistency for the reconstituted Ottawa clay, but represents softer consistency states for mixtures with increasing silt content. Using a fixed void ratio enables direct comparison of the mixtures under an equivalent global packing condition (average dry density $\rho_{dry} \approx 1.53$ g/cm^3), allowing the physical changes with particle shape and aspect ratio to be better evaluated.

Fig. 9 shows the relative variations in G_{max} compared to that of the pure clay ($G_{max\text{-}clay}$), as a function of the particle size ratio, $R_d = d_{50\text{-}mix}/d_{50\text{-}clay}$, where $d_{50\text{-}mix}$ and $d_{50\text{-}clay}$ denote the mean particle sizes of the mixture and the Ottawa clay, respectively. The data used is for $e = 0.8$, providing the intermediate density benchmark. All the mixtures show reductions in relative maximum shear modulus with increasing particle size disparity. The calcite shows the largest range of R_d, whilst the aragonite shows the smallest range. Two tendencies are observed in Fig. 9; the calcite mixtures (pink line) follow approximately the same reductions with increasing R_d as found for the sand-silt mixtures by Li et al. [56], because of the high d_{50} values in the mixture, while the 25% to 60% aragonite mixtures (blue line) have the lowest normalized $G_{max}/G_{max\text{-}clay}$ reduction due to the low R_d values.

This reduction in normalized G_{max} with R_d is related to the interparticle contact stiffness changes between the silt and clay grains and follows the behaviour described by Choo & Burns [60], who found that stiffness reduction in binary mixtures is more pronounced as the size ratio between particles increases, due to greater disruption of force chains among larger particles. Additionally, Wichtmann & Triantafyllidis [61] attributed the reduction of the G_{max} to the presence of strong and weak force chains in mixtures with high coefficient of uniformity, in contrast to uniformly graded soils where force chains are equally distributed. This behaviour is observed in the calcite and silicate mixtures, which shows a lower normalized G_{max} than the aragonite mixtures. Therefore, the slight reduction of the stiffness in the 25% to 60% aragonite mixtures is attributed to their relatively small variation in C_u in comparison to the calcite or silicate mixtures.

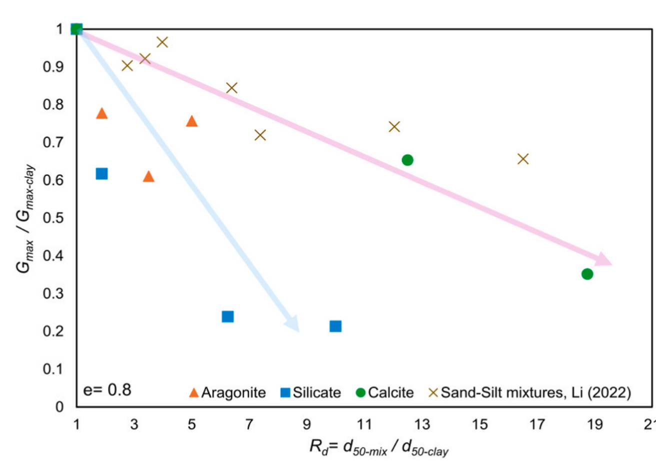

Fig. 9. Normalized $G_{max}/G_{max\text{-}clay}$ with relative particle size ($e = 0.8$).

The influence of grading on small-strain stiffness is further governed by the combined effects of the fine matrix state and the increasing presence of coarse inclusions. At low confining stress and a loose reference state ($e = 0.8$), the introduction of silt disrupts inter-fine grain contacts and weakens the continuity of force chains within the clay matrix, resulting in lower $G_{\max}$ relative to the pure clay. With increasing effective confining stress and associated densification of the matrix, the mechanical contribution of the coarse fraction becomes increasingly significant. Under these denser conditions, coarse particles actively participate in load transfer, leading to a marked increase in $G_{\max}$ with silt content. This transition reflects the development of a more effective force chain network as the proportion of coarse particles increases, in agreement with previous studies on gap-graded soils [62].

4.2.2. Normalized shear modulus $G_{max}/f(e)$

Further normalization of the $G_{\max}$ values can also be conducted using an exponential void ratio function, $f(e) = e^{-1.11}$. This is found to provide shear modulus values consistent with the upper bound of Eastern Canadian clays [8], and this approach is also supported by Lo Presti & Jamiolkowski [16], who applied similar exponential formulations for carbonate soils, where the exponent of the void ratio function decreases with higher carbonate content and reduced clay fractions.

Fig. 10 shows normalized small-strain shear modulus $G_{\max}/f(e)$ values along with data from the literature on silty clays, clayey silts, and sand-silt mixtures. The curves for calcareous clays from the Gulf of Mexico [43] and calcareous silts from the Persian Gulf [63] are found to overlap with the artificial carbonate mixtures at low stresses (<100 kPa), but lie above at higher effective confining stresses. In contrast, silicate mixtures, e.g. Refs. [11,50], and sand-kaolin mixtures [64] fall within the range of the artificial silicate mixtures. Two distinct trends appear in the data set. For silicate and kaolin mixtures, normalized stiffness decreases with increasing silt content, reflecting the reduction in PI and lower clay fractions [48]. In contrast, carbonate mixtures reveal a fundamentally different response: PI ceases to govern the behaviour, and calcium carbonate content becomes the dominant factor. As shown here and by Kallioglou et al. [65], normalized stiffness curves shift upwards with increasing $CaCO_3$ content, and their slopes reflect the combined effects of the carbonate-clay interactions.

To quantify the very small shear modulus behaviour across mixtures, the normalized $G_{\max}/f(e)$ values of the 50% artificial mixtures and other binary sediments were also compared against the reconstituted Ottawa clay at 100 kPa ($G_{\max}/f(e) = 32.37$). The artificial aragonite and calcite mixtures show increases of approximately 34%, while the silicate mixture shows only a 6% increase, confirming the minor contribution of non-plastic silt particles to the stiffness enhancement. Natural and calcareous silts from the Gulf of Mexico and the Persian Gulf [43,63] show 19 - 36% increases, which fall within the range of the artificial carbonate mixtures. The highest increments, from 116% to 215%, correspond to onshore carbonate clays with 38% - 80% $CaCO_3$ and moderate plasticity [65], highlighting the dominant role of carbonate cementation and interparticle bonding in natural onshore carbonate clays [65], where long-term geological processes promote true cemented structures.

4.3. Stiffness degradation

4.3.1. Shear modulus (G) from resonant column tests

Fig. 11 shows the variation of the shear modulus (G) with shear strain for a selection of the undisturbed and reconstituted clay, aragonite and silicate mixtures measured using the resonant column. The G values at small-strains (<0.001%) are consistent with those reported previously for $G_{\max}$ determined with bender elements. With increasing strain, the shear modulus decays in a typical non-linear tendency, highlighting the transition from truly elastic to non-linear elastic response. As shown in the figures, the reconstituted Ottawa clay shows higher shear modulus (G) values compared to the undisturbed sample. Among the artificial samples, the aragonite mixtures consistently show higher G values than the silicate mixtures, reflecting the influence of carbonate particles embedded in the mixtures. A more detailed analysis of the shear modulus degradation and the damping ratio curves is presented in the following sections.

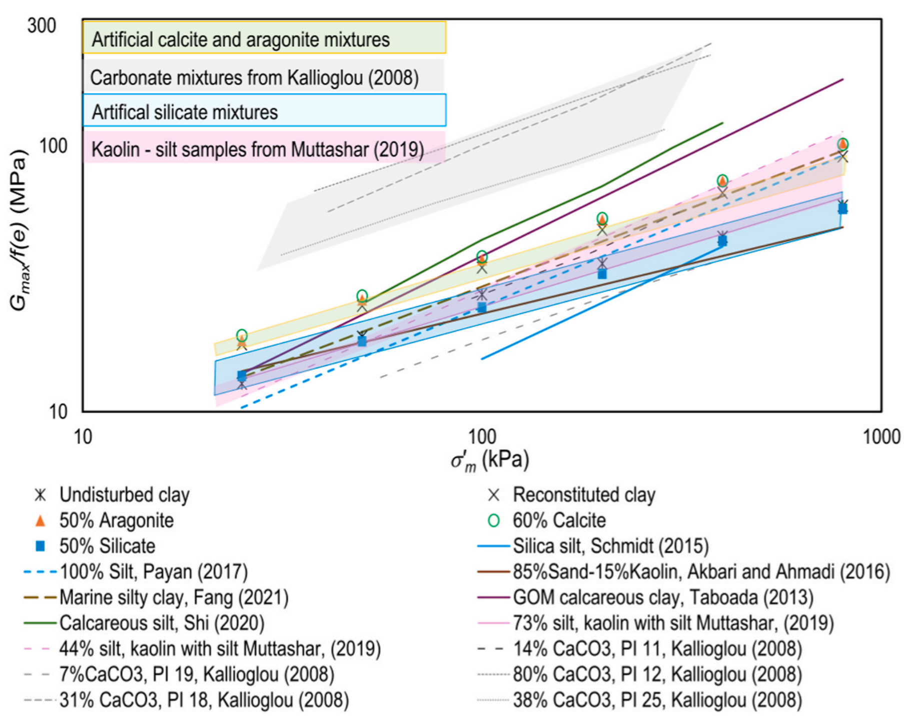

Fig. 10. Normalized $G_{\max}/f(e)$ for the artificial mixtures and literature results.

4.3.2. Stiffness degradation curves (G/G_{max})

Fig. 12 shows the normalized degradation curves (by G_{max}) of various samples tested at 60 kPa confining pressure (OCR $\approx$ 2). The undisturbed Ottawa clay sample response matches that of Leda clay [34] and the upper bound of the Eastern Canadian clays. In contrast, the reconstituted pure clay response shows greater degradation at stiffness ratios below $G/G_{max} < 0.8$ than the undisturbed sample, likely due to the absence of structure. This occurs even though the reconstituted clay sample lies in the range of the stiffer Eastern Canadian clays. It is anticipated that the curves will move to the left with higher silt % and reducing plasticity index. The 50% aragonite mixture exhibits a response comparable to the offshore carbonate clay (OCR = 1.5) from the Gulf of Mexico (GOM) [20]. The GOM clay exhibits a general greater stiffness than the aragonite mixture because its higher PI = 38.6 and its overconsolidated state, as the confining pressures applied during testing ($\sigma_m' \approx 40$ kPa) were below its preconsolidation stress. On the other hand, the 50% silicate mixture falls near the Canadian clay lower bound. Both silt mixtures appear to be influenced by their reductions in plasticity, but the position change for aragonite is much less, which was expected due to the higher PI and the lower coefficient of uniformity [7].

The corresponding curves for $\sigma_m' > 100$ kPa are shown in Fig. 13. Most of the samples show a minor shift to the left for pressure increases from 60 kPa to 300 kPa, likely reflecting partial structural disturbance due to the application of stresses above the preconsolidation level. Such loading may alter the sample, leading to slight reduction in small-strain stiffness. This reduction in the stiffness which is also shown in the reduction in their γ_{ref} from samples tested from an overconsolidated to a normally consolidated soil state has not been extensively studied. Few authors have observed that the stress ratio along the pre-consolidation path significantly influences the stiffness degradation behaviour of cohesive soils in a normally consolidated (NC) state [66,67]. Specifically, the stress history associated with the overconsolidation appears to accelerate the rate of stiffness degradation in NC samples. Interestingly, the aragonite curve essentially maintains its position at 100 and 300 kPa confining stresses. The 50% aragonite mixture behaves similarly to the silt-clay sample as its curve lies in the same range as the 40% silt-clay mixture [68], while the 50% silicate mixture shifts its curve to the right from 100 kPa to 300 kPa and aligns better with the 40% sand and 20% clay.

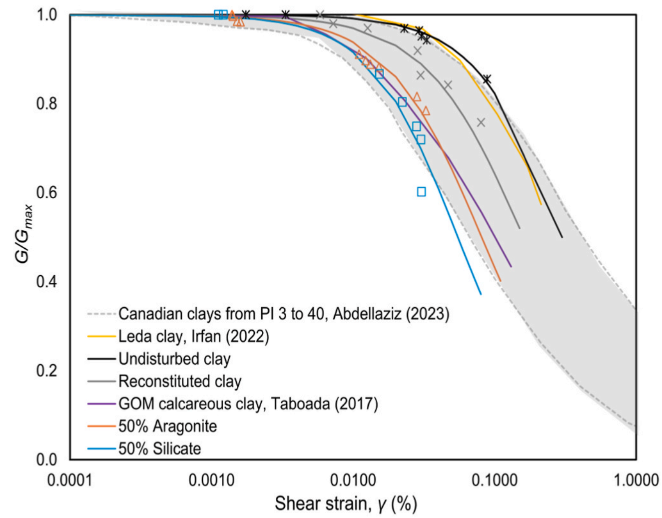

Fig. 12. Stiffness degradation curves of pure clay and artificial mixtures at 60 kPa, OCR $\approx$ 2.

These results suggest the silicate mixtures show behaviour closer to sand-silt or cohesionless sediments, whereas the aragonites resemble more clay-like or cohesive samples, which may be due to crushing occurring, counteracting the silt influence and their lower C_u and higher PI. The effect of plasticity on the threshold strain deserves particular attention. The degradation threshold strain (γ_{ref}) increases with increasing plasticity, reflecting the role of the interparticle electrical forces that stabilize the soil fabric. This behaviour can be rationalized

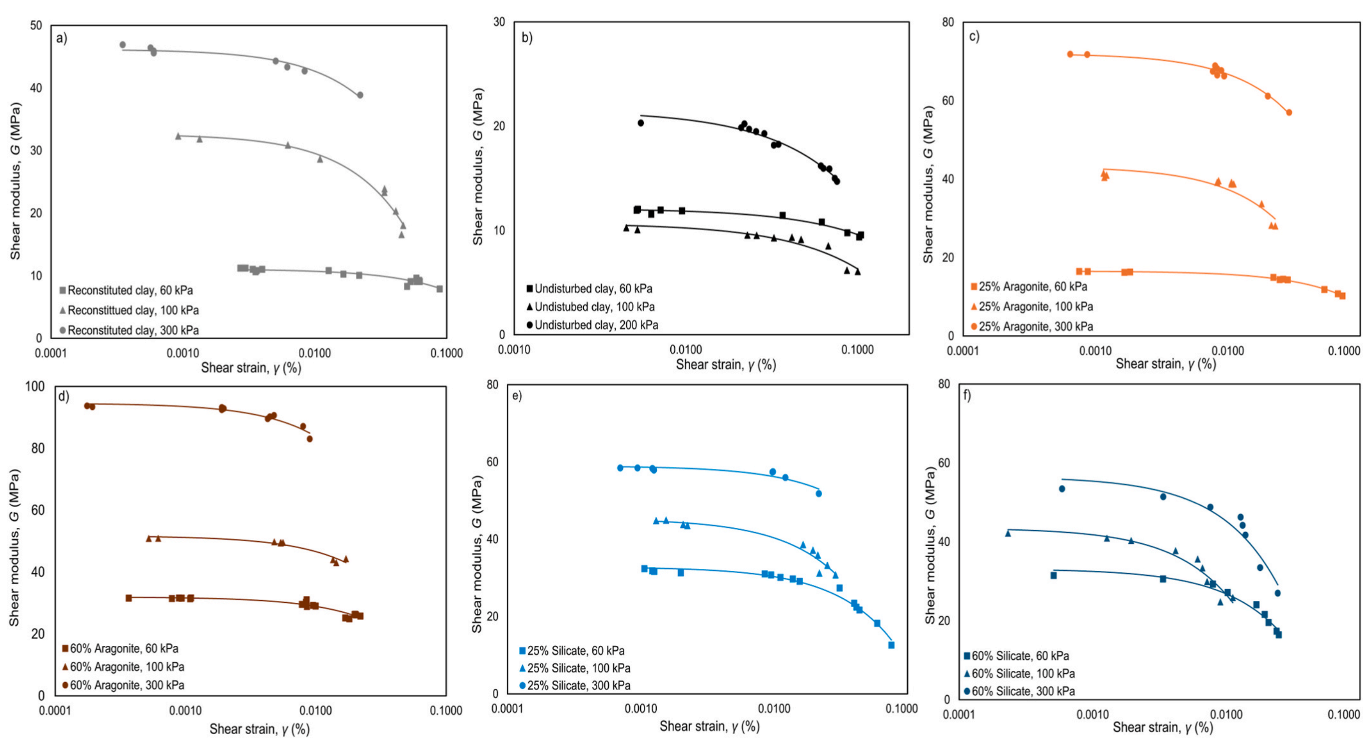

Fig. 11. Shear modulus (G) of undisturbed and reconstituted Ottawa clay, aragonite and silicate artificial mixtures from resonant column testing.

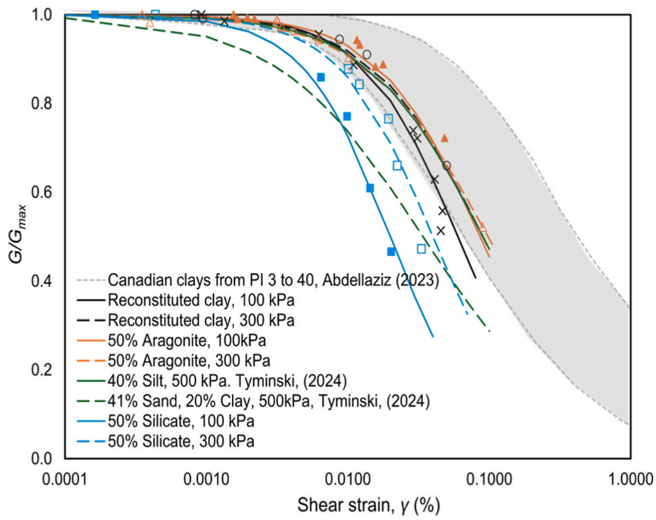

Fig. 13. Stiffness degradation curves for the pure clay and artificial mixtures at stresses >100 kPa.

through the concept of double layer thickness, which increases with PI and particle surface activity [41]. Thus, calcium carbonate mixtures show higher electromechanical attraction compared to inert silicate mixtures, leading to higher γ_{ref}.

4.3.3. Empirical hyperbolic model

Equation (11) is commonly used for normalizing shear modulus behaviour [7]. The shape of the location and hyperbolic model is controlled by the reference strain (γ_{ref}) and curvature parameter (α_γ).

$$G \Big/ G_{max} = 1 \Big/ \left(1 + \gamma \Big/ \gamma_{ref}\right)^{\alpha_\gamma} \tag{11}$$

Where G is the shear modulus, $G_{\max}$ is the shear modulus at very small-strains, γ is the shear strain, γ_{ref} is the reference shear strain (for this study 50% of the $G/G_{\max}$), and α_γ is the curvature parameter.

Table 3 summarizes these parameters for the tested samples, to better quantify these changes. The undisturbed clay shows the highest values of γ_{ref} for both OC and NC soil states, showing the importance of its structure. The reconstituted Ottawa clay shows, the second highest γ_{ref} for the OC condition, while the 50% aragonite shows the second highest γ_{ref} for the NC condition and the silicate mixtures have the lowest γ_{ref} for both soil states. The decrease in γ_{ref} with increasing silt content, connected with higher C_u and lower PI, leads to a corresponding rise in the curvature parameter (α_γ) compared to the reconstituted clay. This behavior is attributed to the illite clay mineral present in Ottawa clay, which effectively enhances stiffness at strains below 0.01%, but exhibits limited contributions at larger strains. Consequently, the silicate mixtures with higher C_u and lower PI experience more rapid stiffness degradation, resulting in greater initial curvature (α_γ) compared to the aragonite mixtures.

Fig. 14 shows the reference strain (γ_{ref}) and curvature (α_γ) parameters as functions of coefficient of uniformity of the reconstituted clay and the artificial aragonite and silicate mixtures, evaluated at three different effective confining stresses. The reference strain results show a clear decreasing trend with increasing C_u, consistent with the behaviour reported for quartz sands by Wichtmann & Triantafyllidis [69], who reported a power-law relationship for granular soils. This behaviour can be attributed to the effect of particle gradation on the evolution of the internal fabric under small-strain dynamic loading. As the coefficient of uniformity increases, the contact network becomes progressively more heterogeneous, with load transfer concentrated through a reduced number of dominant contacts. Under cyclic deformation, this fabric promotes earlier development of localized strains at the particle scale, leading to a more pronounced stiffness degradation at a given strain level. Consequently, the characteristic reference strain decreases with increasing C_u [61,69]. However, the values obtained for the artificial mixtures are higher, reflecting the greater strain performance of the Ottawa clay matrix and its cohesive nature. This trend is expected, as cohesive fine-grained materials typically show larger reference strains than non-plastic silts or clean sands [18,19]. In contrast, the curvature parameter α_γ remains relatively constant ($\alpha_\gamma \approx 1.3$) across the different coefficients of uniformity due to its limited variation with grading [69].

Although C_u, R_d, and PI are not strictly independent parameters, the experimental results show that their respective influences on the dynamic response can be consistently interpreted. In general, increases in C_u and R_d lead to reductions in $G_{\max}$ and reference strain due to increased fabric heterogeneity and disruption of force chain contacts. However, this effect is modulated by physicochemical interactions associated with the plasticity index. In the present study, aragonite mixtures exhibit higher PI and lower C_u than the silicate mixtures, resulting in higher $G_{\max}$ and reference strains under comparable grading conditions. While both artificial mixtures show decreasing $G_{\max}$ and γ_{ref} with increasing C_u, the reduction is more pronounced for the silicate mixtures due to their higher C_u and lower PI. This indicates that, although grading controls the overall trend, plasticity governs the resistance of the soil fabric to stiffness degradation. Higher plasticity increases the interparticle electrical interaction range and degradation threshold strain, thereby reducing the susceptibility of force chains to buckling and instability [41]. Consequently, the dynamic behaviour of the aragonite mixtures reflects a coupled but interpretable interaction between grading and physicochemical effects, with PI partially compensating for fabric heterogeneity associated with grading.

4.3.4. Comparative results with other silty clay sediments

Fig. 15 shows the results of the reconstituted Ottawa clay, and 50% aragonite and silicate mixtures tested at 300 kPa, with, some degradation curves from other researchers to corroborate the experimental results of this research. Shan et al. [70] demonstrate the importance of the clay mineral in the stiffness degradation curves, with their

Table 3
Reference strain and curvature parameters.

Sample	σ_m' (kPa)	γ_{ref}	α_γ	R^2	Sample	σ_m' (kPa)	γ_{ref}	α_γ	R^2
Undisturbed Ottawa clay	60	0.300	1.40	0.98	Reconstituted Ottawa clay	60	0.16	1.25	0.92
	100	0.090	1.50	0.91		100	0.06	1.30	0.97
	200	0.200	1.20	0.96		300	0.09	1.10	0.96
25% silicate	60	0.075	1.30	0.97	25% aragonite	60	0.11	1.30	0.98
	100	0.055	1.30	0.95		100	0.07	1.30	0.89
	300	0.10	1.50	0.85		300	0.08	1.25	0.97
50% silicate	60	0.055	1.40	0.93	50% aragonite	60	0.081	1.30	0.97
	100	0.040	1.30	0.86		100	0.086	1.20	0.92
	300	0.050	1.40	0.93		300	0.098	1.00	0.91
60% silicate	60	0.030	1.50	0.96	60% aragonite	60	0.060	1.30	0.94
	100	0.015	1.40	0.95		100	0.070	1.30	0.93
	300	0.030	1.40	0.92		300	0.085	1.11	0.92

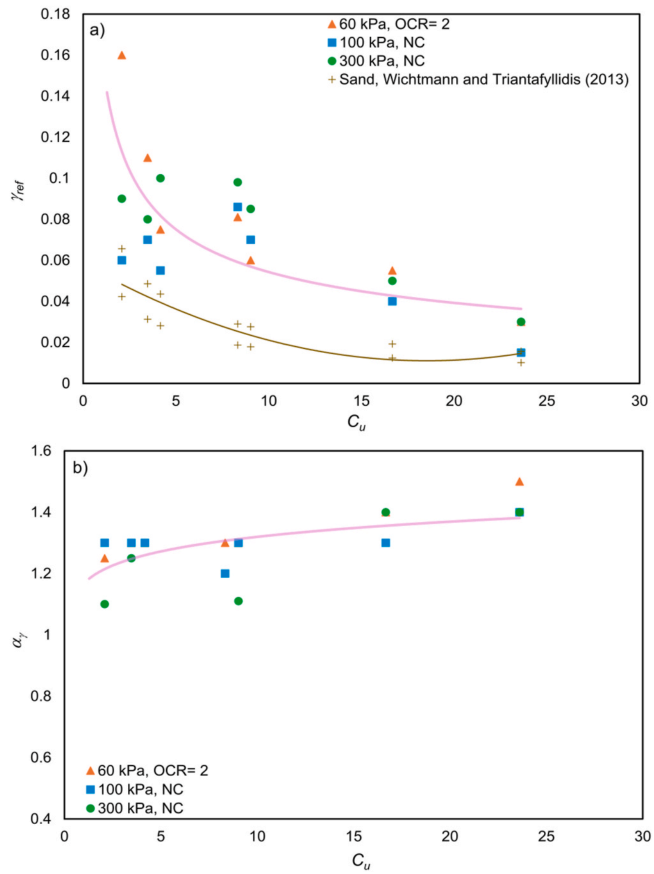

Fig. 14. Strain reference (γ_{ref}) and curvature parameters (α_γ) of artificial mixtures.

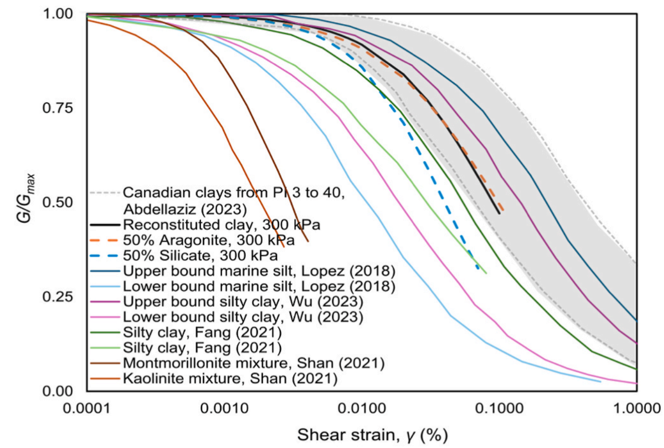

Fig. 15. Stiffness degradation curve artificial mixtures at 300 kPa and marine sediments from literature.

montmorillonite-silt mixtures having higher stiffness and more curvature at smaller strains $\gamma < 0.001\%$ than the kaolinite-silt mixtures, suggesting that more active clay minerals increase the curvature of the degradation curve, while the plasticity increases the reference strain. Considering this conclusion and the stiffness behaviour of the Eastern Canadian clays, for the Ottawa clay, silicate and aragonite artificial mixtures, the pronounced curvature observed in their stiffness degradation curves at non-linear strain levels is consistent.

Furthermore, the 50% silicate mixture and 60% aragonite mixture lie above the average results of the silt and silty clay, respectively, from undisturbed marine samples tested by Fang et al. [46]. In that study, the silty clays (PI between 10 and 15) showed higher stiffness degradation curves than the silts (PI < 10), reflecting the influence of plasticity. A similar tendency is exhibited with the aragonite and silicate mixtures, where the aragonite mixtures with higher plasticity lies above the silicate mixtures in the degradation curves. The 50% artificial mixtures show higher curvature than previous marine sediments and cohesionless carbonate silt sediments from the GOM and according to more extensive experimental research from more undisturbed marine soils on the east coast of China [71] and silt sediments from the GOM [72]; the artificial mixtures lie in the range of both marine sediments.

To facilitate a quantitative comparison between the mixtures and the literature data, all reference strain values from the literature and those from the reconstituted samples (clay, aragonite, and silicate) were evaluated at a mean effective confining stress of 100 kPa. At an effective confining pressure of 100 kPa, the reconstituted clay shows normalized stiffness ratios ($G/G_{\max}$) of 0.96 and 0.80 at 0.005% and 0.002% shear strain, respectively. The 50% aragonite mixture shows no stiffness reduction at 0.005% and a slight increase (6%) at 0.02%. On the other hand, the 50% silicate mixture shows a significant stiffness reduction of approximately −8.9% and −37.5% at the same strain levels, similar to sandy silty clay [68], which shows reductions of −14.1% and −25%, respectively. The stiff calcareous clay from the GOM [20] does not show stiffness degradation at 0.005% shear strain, but shows a 12.5% increase at 0.02%, highlighting its stiff behaviour. These observations collectively indicate that the inclusion of calcium carbonate grains enhances the stiffness retention within the clay matrix.

4.4. Damping ratio (D)

Fig. 16 shows the damping ratio, D (%), curves of the undisturbed and reconstituted samples tested at 60 kPa (OCR ≈ 2). The undisturbed clay sample shows the lowest damping because of its high structuration and void ratio, and the silicate mixture has the highest damping ratio due to the lowest PI. The 50% aragonite mixture lies between the undisturbed and silicate results, and its damping ratio curve is slightly higher than the GOM calcareous clay, which is stiffer and produces more damping. Fig. 17 shows the damping ratio of the undisturbed clay sample and reconstituted clay sample at three different stresses. The lowest damping ratios are attributed to its natural structuration and high void ratio, the results lie near the lower boundary of the sensitive Eastern Canada clay envelope proposed by Abdellaziz et al. [73]. In contrast, the reconstituted sample shows higher damping, reinforcing the influence of destructuration on the dynamic behavior.

Fig. 18 shows the damping ratio, D (%), behaviour of artificial aragonite and silicate mixtures, tested under different effective confining stresses (60, 100 and 300 kPa), plotted alongside empirical curves proposed by Wichtmann & Triantafyllidis [69] and Taboada [20]. Wichtmann & Triantafyllidis [69] model is based on the coefficient of uniformity (C_u), showing the effects of particle gradation and Taboada [20] model correlates damping with the plasticity index (PI), reflecting the influence of clay mineralogy and soil plasticity on energy dissipation.

The aragonite mixtures fall slightly below the cohesionless sand predictions from Wichtmann's model, suggesting that the Ottawa clay in the mixtures plays a moderating role in reducing damping. The trends indicate that lower PI and higher C_u contribute to increased damping in these artificial mixtures. Silicate mixtures show a similar tendency to aragonite mixtures. When comparing both models to the laboratory data obtained from resonant column tests, it appears that the model based on C_u provides a better characterization of the artificial mixtures. The predictions from Wichtmann's equation align more closely with the measured damping ratios, suggesting that particle gradation plays a dominant role in governing the damping ratios instead of the plasticity index. Overall, the relatively low damping ratios observed in the

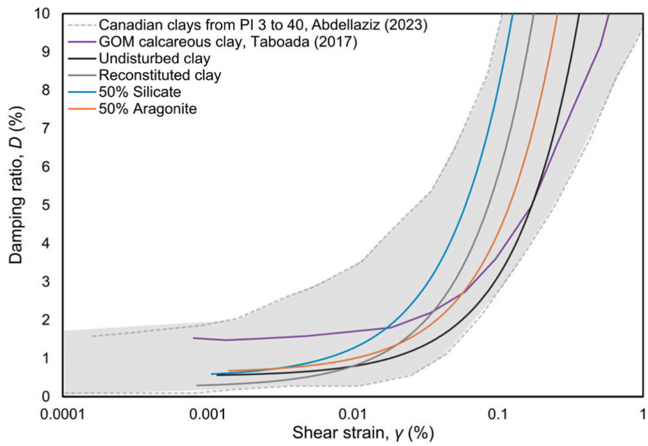

Fig. 16. Damping ratio of 50% artificial mixtures and Ottawa clay samples (OCR $\approx$ 2).

reconstituted and artificial samples can be primarily attributed to the inherent properties of Ottawa clay, emphasizing the critical role of particle grading, and plasticity in controlling dynamic energy dissipation. Additionally, the damping values obtained through the free-decay method can vary due to factors such as signal attenuation, and the assumption of constant exponential decay [74].

Additionally, the damping trends observed in this study reflect the combined effects of particle grading and plasticity on contact kinematics and energy dissipation. In binary mixtures, increasing C_u promotes a shift from sliding to rolling contacts of finer particles, which tends to reduce energy loss and partially compensates for the effect of increased particle size contrast associated with higher C_u values [69]. At larger small-strain levels, soils with lower plasticity exhibit higher damping due to earlier onset of nonlinearity and increased interparticle slip within the contact network. In contrast, soils with higher plasticity maintain a more stable contact response over a wider strain range, as electrochemical interactions associated with fine particles promote flexible yet persistent contacts that delay force chain instability [18,41]. These mechanisms explain the observed moderation of grading effects by plasticity and mineralogy in the damping behaviour, where aragonite mixtures show lower damping than silicate mixtures, and the undisturbed Ottawa clay exhibits the lowest damping as a result of its intact natural structure. At comparable global void ratios, silicate mixtures are expected to develop a less stable contact network with lower effective coordination, allowing greater local rearrangement and interparticle

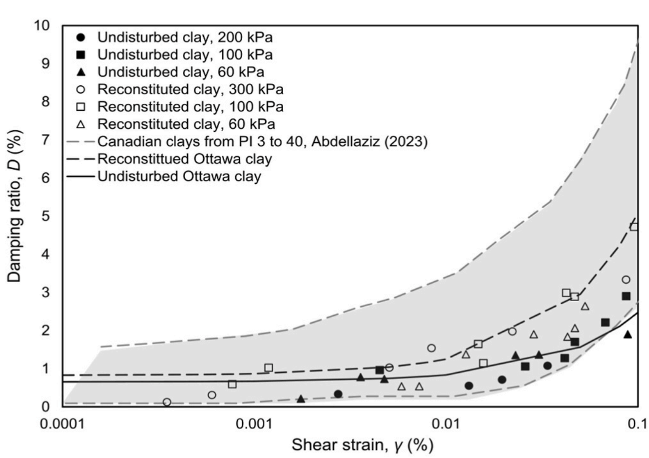

Fig. 17. Damping ratio of Ottawa clay samples at three different confining stresses.

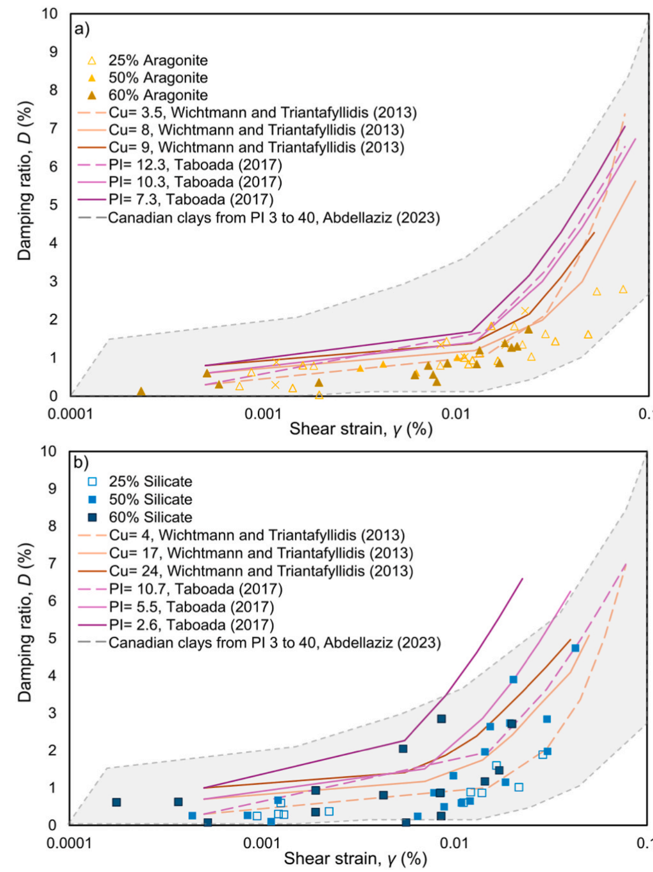

Fig. 18. Damping ratio of artificial mixtures with predictions from empirical equations.

slip, which contributes to the higher damping observed in these mixtures.

5. Conclusions

This study investigates the dynamic behavior and small-strain of artificial marine soils composed of aragonite, calcite and silicate silt mixed with lacustrine clay. Through resonant column and bender element testing under controlled laboratory conditions, this investigation evaluates key dynamic parameters such as the shear wave velocity (v_s), small-strain shear modulus (G_{max}), stiffness degradation (G/G_{max}) and damping ratio (D). The results provide insights into the effect of mineralogy, grain size distribution, and fabric on stiffness and damping, offering a basis for improving the design of structures in offshore carbonate sediments.

The results reveal several notable trends in the dynamic behaviour of the artificial mixtures, as outlined below.

- The artificial mixtures reproduced the small-strain stiffness trends of offshore marine sediments, with calcium carbonate mixtures matching the behaviour of moderate plasticity marine clays. These artificial mixtures also fall within the stiffness degradation range of documented offshore sediments.
- Shear wave velocities (v_s) were consistently higher in the reconstituted Ottawa clay samples compared to undisturbed samples, primarily due to lower void ratios and denser particle contacts from the slurry consolidation process. Calcium carbonate mixtures showed higher v_s values than silicate mixtures, reflecting the impact of mineralogy on wave propagation. This behaviour is attributed to

the role of Ca^{2+} ions, which enhances thickness physicochemical, non-frictional interactions by contracting the diffuse double layer.
- Aragonite mixtures showed the stiffest responses overall, attributed to their lower coefficient of uniformity and non-frictional bonding, which enhanced effective stress transmission through well formed force chains. Calcite mixtures showed lower stiffness, and silica mixtures the lowest, behaving more like cohesionless silts due to its less plasticity index and high coefficient of uniformity.
- Stiffness degradation curves for both undisturbed and reconstituted Ottawa clay samples aligned well with trends observed in other lacustrine and marine clays. Reference strains and damping ratios were notably higher and lower, respectively, in undisturbed samples than reconstituted samples, emphasizing the influence of soil structure on stiffness degradation and energy dissipation.
- Stiffness degradation curves (G/G_{max}) showed a clear dependence on the coefficient of uniformity (C_u) of the silt fraction: as C_u increased, the reference strain decreased, indicating an earlier inflection of stiffness degradation curve. However, mixtures with high Ottawa clay content retained higher initial stiffness at very small-strains, behaving more like structured marine clays.
- Damping ratios (D) were lowest in the aragonite mixtures and highest in silicate mixtures. This pattern aligns with the observed trends in stiffness and suggests that mineralogy, grain shape, and the plasticity of the clay matrix control energy dissipation at small and intermediate strains.

In summary, this research highlights the importance of understanding the interplay between soil fabric, carbonate content, and grain sizes in shaping the dynamic properties of soils. The distinctions between aragonite and calcite mixtures with silicate mixture comparisons provide new insights into the expected behavior of carbonate sediments, contributing to potentially improved design methodologies for offshore foundations and other marine infrastructure projects in the Gulf of Mexico and other challenging offshore carbonate zones. It should be stressed that the interpretations presented in this study are based on laboratory testing of reconstituted and artificial mixtures under a limited range of effective stresses and controlled boundary conditions. As such, the results are intended to capture fundamental mechanisms governing small-strain stiffness and damping in shallow marine sediments, rather than the full response of deep offshore deposits where higher stress levels, stress history, and long-term fabric evolution may become dominant. Accordingly, the findings should be interpreted as mechanistic trends, rather than as direct predictors of in situ performance and further study is required to create materials that are more direct analogs of offshore sediments.

CRediT authorship contribution statement

Alain Conrado-Palafox: Writing – original draft, Visualization, Methodology, Data curation, Conceptualization. **Timothy Newson:** Writing – review & editing, Supervision, Conceptualization.

Statement of originality

The dynamic properties of fine-grained soils are generally described through empirical models developed for terrigenous sediments. However, very limited research has focused on carbonate mixtures, despite their relevance in offshore foundation design. The present study provides new empirical data from resonant column and bender element readings on reconstituted clay and artificial mixtures with controlled proportions of silicate and carbonate silt. The results highlight how mineral inclusions modify plasticity, compressibility, small-strain stiffness and damping, offering insights into the role of carbonate grains in the dynamic response of fine-grained soils.

Declaration of competing interest

The authors declare that they have no known competing financial interests or personal relationship that could have appeared to influence the work reported in this paper.

Acknowledgement

The authors gratefully acknowledge the scholarship provided by the CONAHCYT (Consejo Nacional de Humanidades Ciencias y Tecnologias).

Data availability

Data will be made available on request.

References

[1] Hardenberg M, Vrettos C. Dynamic stiffness and damping of four compacted clays at different consistencies from resonant column tests. Soil Dynam Earthq Eng 2025; 196:109436. https://doi.org/10.1016/j.soildyn.2025.109436.
[2] Shafiee A, Zamanian M, Payan M, Tajani SB, Hassanipour A, Chenari RJ. Strain-dependent dynamic properties of compacted clay-sand mixtures. Soil Dynam Earthq Eng 2025;196:109455. https://doi.org/10.1016/j.soildyn.2025.109455.
[3] Hardin BO, Black WL. Vibration modulus of normally consolidated clay. J Soil Mech Found Div 1968;94(2):353–69. https://doi.org/10.1061/jsfeaq.0001100.
[4] Hardin BO, Black WL. Closure to "Vibration modulus of normally consolidated clay". J Soil Mech Found Div 1969;95(6):1531–7. https://doi.org/10.1061/jsfeaq.0001364.
[5] Hardin BO, Drnevich VP. Shear modulus and damping in soils: measurement and parameter effects. J Soil Mech Found Div 1972;98(6):603–24. https://doi.org/10.1061/jsfeaq.0001756.
[6] Hardin BO, Drnevich VP. Shear modulus and damping in soils: design equations and curves. J Soil Mech Found Div 1972;98(7):667–92. https://doi.org/10.1061/jsfeaq.0001760.
[7] Darendeli M. Development of a new family of normalized modulus reduction and material damping curves. The University of Texas at Austin; 2001. PhD Thesis, http://hdl.handle.net/2152/10396.
[8] Elbeggo D, Ethier Y, Karray M, Dubé JS. Assessment of existing Vs-Lab correlations regarding Eastern Canadian clays. Soil Dynam Earthq Eng 2023;164:107607. https://doi.org/10.1016/j.soildyn.2022.107607.
[9] Cha M, Santamarina JC, Kim HS, Cho GC. Small-strain stiffness, shear-wave velocity, and soil compressibility. J Geotech Geoenviron Eng 2014;140(10). https://doi.org/10.1061/(asce)gt.1943-5606.0001157.
[10] Cascante G, Santamarina JC. Interparticle contact behavior and wave propagation. J Geotech Eng 1996;122(10):831–9. https://doi.org/10.1061/(asce)0733-9410(1996)122:10(831.
[11] Payan M, Senetakis K, Khoshghalb A, Khalili N. Characterization of the small-strain dynamic behaviour of silty sands; contribution of silica non-plastic fines content. Soil Dynam Earthq Eng 2017;102:232–40. https://doi.org/10.1016/j.soildyn.2017.08.008.
[12] Boulanger R, Idriss I. Liquefaction susceptibility criteria for silts and clays. J Geotech Geoenviron Eng 2006;132(11):111413. https://doi.org/10.1061/ASCE1090-02412006132.
[13] Seed R, Cetin K, Moss R. Recent advances in soil liquefaction engineering and seismic site response evaluation. In: Proc of the Fourth international conference on recent advances in Geotech Earthq Eng Soil Dynam and symp in honor of W.D. Liam Finn; 2001.
[14] Stark T, Vettel J, Fitzwilliam M, Ebeling R. Soil structure interaction parameters for silts. Washington: Prepared for US Army Corps of Engineers; 1991. ITL-91-2.
[15] Jamiolkowski M, Lancellotta R, Lo Presti DCF. Remarks on the stiffness at small strains of six Italian clays. Pre-Failure Deformation Charact of Geomaterials 1995: 817–36.
[16] Lo Presti DCF, Jamiolkowski M. Discussion: estimate of elastic shear modulus in Holocene soil deposits. Soils Found 1998;38:263–5.
[17] Lo Presti DCF, Jamiolkowski M, Pallara O, Cavallaro A, Pedroni S. Shear modulus and damping of soils. Geotechnique 1997;47(3):603–17. https://doi.org/10.1680/geot.1997.47.3.603.
[18] Vucetic M, Dobry R. Effect of soil plasticity on cyclic response. J Geotech Eng 1991; 117:89–107. https://doi.org/10.1061/(ASCE)0733-9410(1991)117:1(89.
[19] Vardanega PJ, Bolton MD. Stiffness of clays and silts: normalizing shear modulus and shear strain. J Geotech Geoenviron Eng 2013;139(9):1575–89. https://doi.org/10.1061/(asce)gt.1943-5606.0000887.
[20] Taboada Danta V, Cruz-Roque D, Flores-Lopez F, Vazquez-Monroy R, Barrera P. Normalised modulus reduction and material damping ratio curves for Bay of Campeche clay. In: Offshore site investigation and geotech, 8th international conference proc; 2017. https://doi.org/10.3723/OSIG17.457.
[21] Watson P, et al. Foundation design in offshore carbonate sediments – building on knowledge to address future challenges. In: XVI Pan-American conference on soil mech Geotech Eng (XVI PCSMGE), technical session #8 "offshore geotechnics; 2019.

[22] Jeanjean P, Zakeri A, Zhang Y, Anderson K. The new ISO/API p-y curves in clays and their reconciliation with the PISA framework. In: Offshore Technology conference; 2022. https://doi.org/10.4043/31860-MS.
[23] Zhu J, Huang M, Shi Z, Shen K. Inclusion of small-strain stiffness in monotonic p-y curves for laterally loaded piles in clay. Comput Geotech 2022;150. https://doi.org/10.1016/j.compgeo.2022.104902.
[24] Futai MM, Haigh SK, Madabhushi GSP. Comparison of the dynamic responses of monopiles and gravity base foundations for offshore wind turbines in sand using centrifuge modelling. Soils Found 2021;61(1):50–63. https://doi.org/10.1016/j.sandf.2020.10.009.
[25] Richard A, Davis J. Sediments of the Gulf of Mexico. In: Habitats and biota of the Gulf of Mexico: before the deepwater horizon oil spill; 2017. https://doi.org/10.1007/978-1-4939-3447-8.
[26] Yu J, Yu J, Zhang L, Wang X, Wu L. Facile fabrication and characterization of hierarchically porous calcium carbonate microspheres. Chem Commun 2004;21:2414–5. https://doi.org/10.1039/b406839d.
[27] Conrado-Palafox A, Newson T, Ahmed A. Compressibility transition between a marine onshore clay to artificial carbonate silt soil behaviour. In: 24 Geotech Eng challenges to meet Current and emerging needs of Society, ECSMGE; 2024. https://doi.org/10.1201/9781003431749-418.
[28] Ogino T, Kawaguchi T, Yamashita S, Kawajiri S. Measurement deviations for shear wave velocity of bender element test using time domain, cross-correlation, and frequency domain approaches. Soils Found 2015;55(2):329–42. https://doi.org/10.1016/j.sandf.2015.02.009.
[29] Rees S, Le-Compte A, Snelling K. A new tool for the automated travel time analyses of bender element tests. In: Proc of the 18th international conference on soil mech and Geotech Eng; 2013. p. 2843–6.
[30] Yamashita S, Kawaguchi T, Nakata Y, Mikami T, Fujiwara T, Shibuya S. Interpretation of international parallel test on the measurement of G_{max} using bender elements. Soils Found 2009;49(4):631–50. https://doi.org/10.3208/sandf.49.631.
[31] Fonseca A, Ferreira C, Fahey M. A framework interpreting bender element tests, combining time-domain and frequency domain methods. Geotech Test J 2009;32(2).
[32] GDS Instruments. GDS resonant column: the GDS resonant column system handbook. 2015. Hook, U.K.
[33] ASTM D4015-15e1. Standard test methods for modulus and damping of soils by fixed-base resonant column devices. West Conshohocken, PA: ASTM International; 2015.
[34] Irfan M, Cascante G, Basu D, Leboeuf D. Low-strain dynamic characterization of undisturbed Leda clay. Can Geotech J 2022;59(5):631–43. https://doi.org/10.1139/cgj-2020-0758.
[35] Richart FE, Hall JR. Woods RD Vibration of soils and foundations. Prentice Hall; 1970.
[36] Clayton C, Priest J, Bui M, Zervos A, Kim S. The Stokoe resonant column apparatus: effects of stiffness, mass and specimen fixity. Geotechnique 2009;59(5):429–37. https://doi.org/10.1680/geot.2007.00096.
[37] González-Hurtado J. The effect of stiffness anisotropy of a glacial clay of a glacial clay on the y on the behaviour of a shallow wind turbine foundation. University of Western Ontario; 2019. PhD Thesis, https://hdl.handle.net/20.500.14721/29818.
[38] Xu K, Gu X, Hu C, Lu L. Comparison of small-strain shear modulus and Young's modulus of dry sand measured by resonant column and bender-extender element. Can Geotech J 2020;57:1745–53. https://doi.org/10.1139/cgj-2018-0823.
[39] Facciorusso J, Madiai C. On cohesive soil damping estimation by free vibration method in resonant column test. Geotech Test J 2020;43(6):1499–518. https://doi.org/10.1520/GTJ20180241.
[40] Santamarina JC, Klein K, Fam M. Soils and waves: particulate materials behaviour, characterization, and process monitoring. Chichester, UK: Wiley; 2001.
[41] Santamarina JC. Soil Behaviour at the microscale: particle forces. In: Proc. Symp. Soil behaviour and soft ground construction. MIT; 2001.
[42] Arroyo M, Muir Wood D, Greening P. Source near-effects and pulse tests in soil samples. Geotechnique 2003;53(3):337–45. https://doi.org/10.1680/geot.2003.53.3.337.
[43] Taboada Cruz-Roque, Barrera PN, Espinosa E, Carrasco D, Gan KC. Predictive equations of shear wave velocity for bay of Campeche clay. In: Offshore technology conference; 2013. https://doi.org/10.1201/b18442-166.
[44] Ramirez M, Park J, Terzariol M, Jiang J, Santamarinca JC. Shallow seafloor sediments: density and shear wave velocity. J Geotech Geoenviron Eng 2023;149(5). https://doi.org/10.1061/jggefk.gteng-10759.
[45] Lee JS, Lee JY, Kim YM, Lee C. Stress-dependent and strength properties of gas hydrate-bearing marine sediments from the Ulleung Basin, East Sea, Korea. Mar Petrol Geol 2013;47:66–76. https://doi.org/10.1016/j.marpetgeo.2013.04.006.
[46] Fang Y, Lv Y, Zhou X, Peng Y. Experimental study of the engineering mechanical properties of the foundation soil for offshore wind power platforms. Shock Vib 2021. https://doi.org/10.1155/2021/1382740.
[47] Oh TM, Bang ES, Cho GC, Park ES. Estimation of undrained shear strength for saturated clay using shear wave velocity. Mar Georesour Geotechnol 2017;35(2):236–44. https://doi.org/10.1080/1064119X.2016.1140855.
[48] Muttashar WR, Bryson LS, Woolery E. Determining the effects of depositional processes on consolidation behavior of sediment using shear-wave velocity. Mar Georesour Geotechnol 2019;37(9):1032–43. https://doi.org/10.1080/1064119X.2018.1524953.
[49] Park J, Kim SY, Hoang QN, Lee JS. Impact of diatoms on the load-deformation response of marine sediments during drained shear: Small-to-large strain stiffness. Eng Geology 2023;315. https://doi.org/10.1016/j.enggeo.2023.107006.
[50] Schmidt C. Static and dynamic response of silty Toyoura sand with PVA fibre and cement additives. Western University of Ontario; 2015. Meng Thesis, https://hdl.handle.net/20.500.14721/35778.
[51] Lee J, Francisca F, Santamarina JC, Ruppel C. Parametric study of the physical properties of hydrate-bearing sand, silt, and clay sediments: 2. Small-strain mechanical properties. J Geophys Res 2010;115:B11105. https://doi.org/10.1029/2009JB006670.
[52] Ku T, Subramanian S, Moon S, Jung J. Stress dependency of shear wave velocity measurements in soils. J Geotech Geoenviron Eng 2016;143(2). https://doi.org/10.1061/(ASCE)GT.1943-5606.0001592.
[53] Fam M, Santamarina JC. Study of clay-cement slurries with mechanical and electromagnetic waves. J Geotech Eng 1996;122(5):365–73. https://doi.org/10.1061/(ASCE)0733-9410(1996)122:5(365.
[54] Kang X, Kang G, Bate B. Measurement of stiffness anisotropy in kaolinite using bender element tests in a floating wall consolidometer. Geotech Test J 2014;37(5). https://doi.org/10.1520/GTJ20120205.
[55] Santamarina JC, Cho G. Soil behaviour: the role of particle shape. In: Proc skempton conference; 2004.
[56] Li Y, Otsubo M, Ghaemi A, Dutta TT, Kuwano R. Transition of gap-graded soil fabric – shear wave measurements and dispersion relation. Soils Found 2022;62(1). https://doi.org/10.1016/j.sandf.2021.101092.
[57] Thevanayagam S, Shenthan T, Mohan S, Liang J. Undrained fragility of clean sands, silty sands, and sandy silts. J Geotech Geoenviron Eng 2002;128(10):849–59. https://doi.org/10.1061/~ASCE!1090-0241~2002!128:10~849.
[58] Zhou E, Bai Y, Zou X. Evaluation of dynamic behaviour of rubber particle-clay mixtures using the skeleton void ratio approach. Constr Build Mater 2024;426:136127. https://doi.org/10.1016/j.conbuildmat.2024.136127.
[59] He SH, Goudarzy M, Ding Z, Sun Y, Xu T, Zhang QF. Small-strain shear modulus (G_{max}) and microscopic pore structure of calcareous sand with different grain size distributions. Granul Matter 2022;24(112). https://doi.org/10.1007/s10035-022-01270-2.
[60] Choo H, Burns S. Shear wave velocity of granular mixtures of silica particles as a function of finer fraction, size ratios and void ratios. Granul Matter 2015;17:567–78. https://doi.org/10.1007/s10035-015-0580-2.
[61] Wichtmann T, Triantafyllidis T. On the influence of the grain size distribution curve on dynamic properties of quartz sand. In: Fifth international conference on recent advances in Geotech Earthq Eng Soil Dynam; 2010.
[62] Shi XS, Nie J, Zhao J, Gao Y. A homogenization equation for the small strain stiffness of gap-graded granular materials. Comput Geotech 2020;121:103440. https://doi.org/10.1016/j.compgeo.2020.103440.
[63] Shi J, Haegeman W, Xu T. Effect of non-plastic fines on the anisotropic small strain stiffness of a calcareous sand. Soil Dynam Earthq Eng 2020;139:106381. https://doi.org/10.1016/j.soildyn.2020.106381.
[64] Akbari PN, Ahmadi MM. Effect of fines type and content of sand on correlation between shear wave velocity and liquefaction resistance. Geotech Geological Eng 2016;34(6):1857–76. https://doi.org/10.1007/s10706-016-9995-8.
[65] Kallioglou P, Tika T, Pitilakis K. Erratum: shear modulus and damping ratio of cohesive soils. J Earthq Eng 2008;12(6):879–913. https://doi.org/10.1080/13632460802536552.
[66] Butcher A, Powell J. Deformation properties of soil from in situ and laboratory tests. In: 15th international conference on soil mech and found Eng; 2001.
[67] Choo J, Jung YH, Cho W, Chung CK. Effect of pre-shear stress path on nonlinear shear stiffness degradation of cohesive soils. Geotech Test J 2013;36(2). https://doi.org/10.1520/GTJ20120116.
[68] Tyminski W, Kiełczewski T, Stajszczak P. The influence of clay and silt content on reducing stiffness of soil in a small range of strains. In: 24 Geotech Eng challenges to meet Current and emerging needs of Society, ECSMGE; 2024. https://doi.org/10.1201/9781003431749-154.
[69] Wichtmann T, Triantafyllidis Th. Effect of uniformity coefficient on G/G_{max} and damping ratio of uniform to well graded quartz sands. J Geotech Geoenviron Eng 2013;139(1):59–72. https://doi.org/10.1061/(ASCE)GT.1943-5606.0000735.
[70] Shan Y, Wang X, Cui J, Mo H, Li Y. Effects of clay mineral composition on the dynamic properties and fabric of artificial marine clay. J Marine Science Eng 2021;9(1216). https://doi.org/10.3390/jmse9111216.
[71] Wu Q, Xiao X, Zhu E, Chen S, Chen G, Du X. Experimental investigation on dynamic shear modulus of undisturbed marine soils in the east coast of China. Ocean Eng 2023;289. https://doi.org/10.1016/j.oceaneng.2023.116130.
[72] Lopez F, Taboada Ramirez Z, Roque DC, Nabor PB, Dantal VS. Normalized modulus reduction and damping ratio curves for Bay of Campeche carbonate sand. In: Proc of the annual offshore technology conference; 2018. https://doi.org/10.4043/29010-ms. OTC-29010-MS.
[73] Abdellaziz M, Karray M, Chekired M, Delisle MC, Ledoux C, Mompin R. New model of shear modulus degradation and damping ratio curves for sensitive Canadian clays. Can Geotech J 2023;60(6):784–801. https://doi.org/10.1139/cgj-2021-0475.
[74] Mog K, Anbazhagan P. Evolution of the damping ratio of soils in a resonant column using different methods. Soils Found 2022;62(1):101091. https://doi.org/10.1016/j.sandf.2021.101091.